Research of Lithium Iron Phosphate as Material of Positive Electrode of Lithium-Ion Battery

A.A. Chekannikov[1], R.R. Kapaev[2], S.A. Novikova[2], T.L.Kulova[1,], A.M. Skundin[1], A.B. Yaroslavtsev[2]*

[1]Frumkin Institute of Physical Chemistry and Electrochemistry of the RAS, 31-4 Leninskii prosp., 119071 Moscow, Russia
[2] Kurnakov Institute of General and Inorganic Chemistry of the RAS, 31 Leninskii prosp., 119071 Moscow, Russia
[*]E-mail: tkulova@mail.ru

In the present paper, samples of pure and doped lithium iron phosphate composite with the following composition: $LiFePO_4/C$, $Li_{0.99}Fe_{0.98}(CrNi)_{0.01}PO_4/C$ were synthesized. The samples were synthesized using the sol-gel method. According to the acquired data, all the obtained samples of lithium iron phosphate are crystallized in the orthorhombic modification of lithium iron phosphate with the structure of olivine. The average particle size of the obtained materials varies in the range of 50-100 nm. The carbon content was 4 wt%. The doping of lithium iron phosphate with trivalent cations of chromium and nickel results in the increase of the discharge capacity at high discharge rates with the simultaneous stability augmentation during the cycling.

1. INTRODUCTION

Materials based on lithium iron phosphate are being widely used for positive electrodes of lithium-ion batteries. The main disadvantage of $LiFePO_4$ (its low electronic conductivity) was eliminated through the synthesis of the lithium iron phosphate composite with carbon ($LiFePO_4/C$) [1 - 4]. The synthesis of $LiFePO_4$ composites with carbon allows increasing the electronic conductivity by several orders of magnitude [5-8]. Further increase of electronic conductivity can be reached through the synthesis of doped $LiFePO_4/C$ composites. Ions of transition metals, such as Mn [9, 10, 11], V [12, 13, 14], Mg [15, 16], Ni [17], Co [18], Mo [19], La [20], Gd [21], Cr [22] can act as dopants. Further increase of electronic conductivity will allow using doped $LiFePO_4/C$ at forced and pulse loads.

2. EXPERIMENTAL METHODS AND MATERIALS

For the synthesis of lithium iron phosphate samples doped with trivalent cations of nickel and chromium ($Li_{0.99}Fe_{0.98}(CrNi)_{0.01}PO_4/C$) with the structure of olivine, Li_2CO_3, $Fe(NO_3)_3 \cdot 9H_2O$, $(NH_4)_2HPO_4$, $Cr(NO_3)_3 \cdot 9H_2O$ $Ni(NO_3)_{2*}6H_2O$ were used. The synthesis was conducted using the sol-gel method. At the first stage, reagents were mixed in stoichiometric ratios in deionized water. The obtained solution was exposed at 70°C for 4 hours with constant stirring to obtain homogeneous suspension. The obtained suspensions were exposed to drying with subsequent annealing in an argon atmosphere at 800°C. As a result, crystalline products of required composition with the structure of olivine were obtained.

To obtain composite materials with carbon based on $Li_{1-x}Fe_{1-2x}Ni_xCr_xPO_4$ (x=0; 0.01), lithium iron phosphate samples were ground with glucose with post-heat treatment at 800°C in an inert atmosphere for 2 hours.

Crystal structure was characterized by X-ray diffraction (XRD) with CuK_α radiation performed on a Rigaku D/MAX 2200 diffractometer. The Rigaku Application Data Processing software package was used for spectra processing. The obtained experimental diffraction patterns were compared with the PDF 2 ICDD diffraction standards database. Lattice parameters were updated using the Checkcell debugging tool. The size of coherent scattering regions (CSR) was calculated from the broadening of diffraction peaks using the Scherrer formula:

$$d = \frac{k\lambda}{(\beta - \beta_0)\cos\theta}$$

(1)

where d is crystallite size, λ is radiation wavelength $\lambda(CuK_\alpha)$ = 1.5406 Å, θ is diffraction angle of peak position (rad.), β is peak width at half-height (rad.), β_0 is instrumental broadening (rad.), k = 0.9 is the Scherrer constant. The instrumental broadening was determined using the LaB_6 standard.

Microstructures and elemental composition of obtained materials were examined with the help of Carl Zeiss NVision 40 scanning electron microscope SEM (micrographs were obtained at an accelerating voltage of 7 kV), equipped with an Oxford Instruments X-MAX energy-dispersive X-ray (EDX) analyzer operating at an accelerating voltage of 30 kV.

Electrodes for electrochemical researches were prepared by a standard paste method. The cathode paste consisted of 85% active material, 10% carbon black and 5% polyvinylidenfluoride dissolved in anhydrous *N*-methylpyrrolidone. A stainless steel mesh with a welded stainless steel wire terminal served as a current collector. Electrochemical cells were assembled in a glove box (SPEKS, Russia) in a dry argon atmosphere. Water and oxygen content in the compartment did not exceed 10 ppm. Electrochemical cells contained one working electrode (lithium iron phosphate composite), one lithium counter electrode and one lithium reference electrode. The mass of active material in the working electrode was 10–15 mg/cm^2. Electrochemical researches were conducted in galvanostatic and potentiodynamic modes. The current density in galvanostatic measurements ranged from 20 to 3200 mA/g. The potential scan rate ranged from 0.1 to 1.0 mV/s. The 1 M $LiPF_6$ solution in a mixture

of ethylene carbonate-diethyl carbonate-dimethyl carbonate (1:1:1) served as an electrolyte. Water content in the electrolyte did not exceed 20 ppm.

3. RESULTS AND DISCUSSION

According to the data of XRD, synthesized materials of $LiFePO_4/C$ and $Li_{0.99}Fe_{0.98}Ni_{0.01}Cr_{0.01}PO_4/C$ compositions are crystallized in the orthorhombic modification of $LiFePO_4$. The fragments of diffraction patterns of obtained materials are presented in Fig. 1. Reflexes on diffraction patterns correlate with those of $LiFePO_4$ (Card No. 81-1173 PDF2 ICDD, triphylite, orthorhombic modification, *Pnma* space group). Reflexes of other phases are not detected. The particle sizes calculated based on XRD results using the Scherrer formula by order of magnitude were 50 nm.
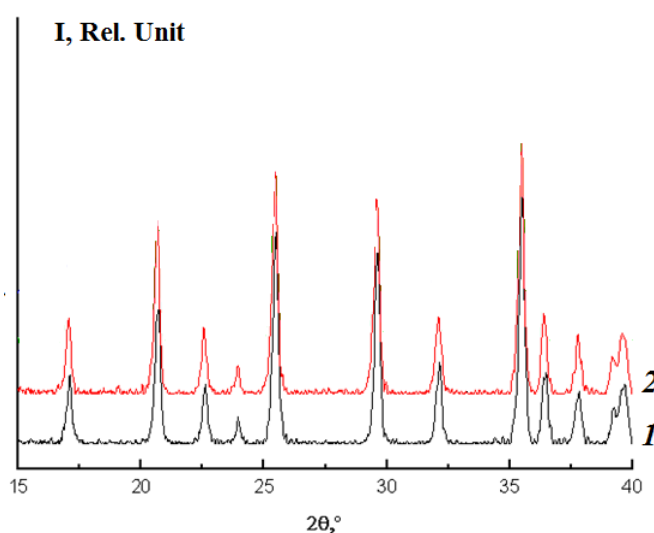
Figure 1. Fragments of diffraction patterns: 1 – $LiFePO_4/C$; 2 – $Li_{0.99}Fe_{0.98}Ni_{0.01}Cr_{0.01}PO_4/C$.

The electron micrographs of the synthesized sample of $LiFePO_4/C$ are presented in Fig. 2. The average size of particles of the $LiFePO_4/C$ composite is 100 nm, whereas there are particles in the material ranging from 50 to 400 nm. A closer look at micrographs shows that there are also individual agglomerates up to 3 µm in the sample (Fig. 2 a, b). The electron micrographs of the $Li_{0.99}Fe_{0.98}Ni_{0.01}Cr_{0.01}PO_4/C$ doped sample are presented in Fig. 3. Morphology of the doped sample is similar to that of $LiFePO_4/C$, at the same time it is established that the doping results in the reduction of agglomerated particles size to 1 µm. The average size of particles of the doped composite is also reduced and is about 50 nm.

The X-ray spectroscopic microanaysis (EDX) of the $Li_{0.99}Fe_{0.98}Ni_{0.01}Cr_{0.01}PO_4/C$ sample showed that the distribution of elements in the structure is even and corresponds to the initial load (Fig. 4 and 5). Fig. 4 shows the sites at which X-ray microanalysis was carried out. The results of EDX along with relative error are presented in Table 1. The EDX result of $Li_{0.99}Fe_{0.98}Ni_{0.01}Cr_{0.01}PO_4/C$ for spectrum 5 (Fig. 5) indicates that the element composition of particle includes Fe, P, O, C, Ni and Cr, thus no other impurity is introduced to the as-prepared samples during the preparation process. The results of EDX at other sites were similar.
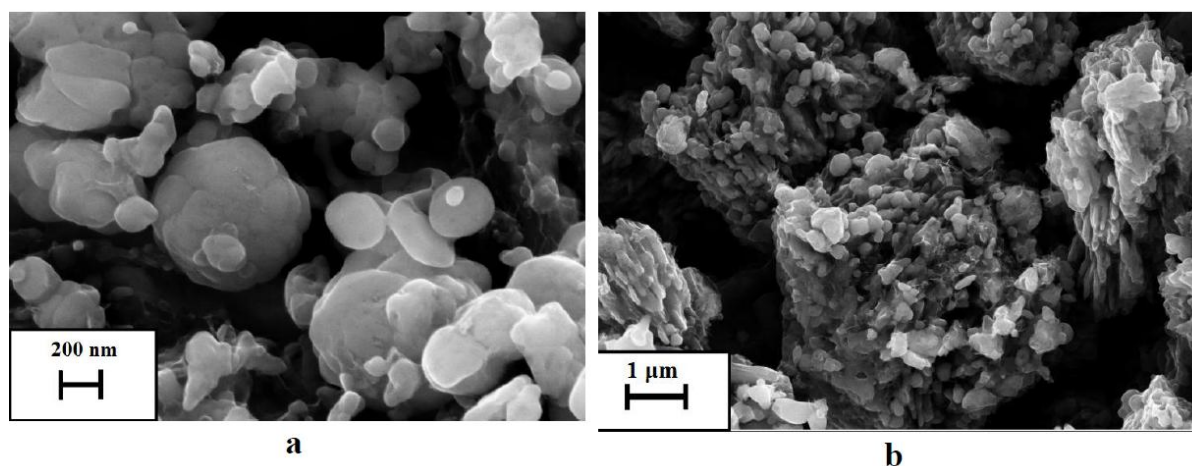
Figure 2. SEM micrographs of LiFePO$_4$/C taken at different magnification (a, b).
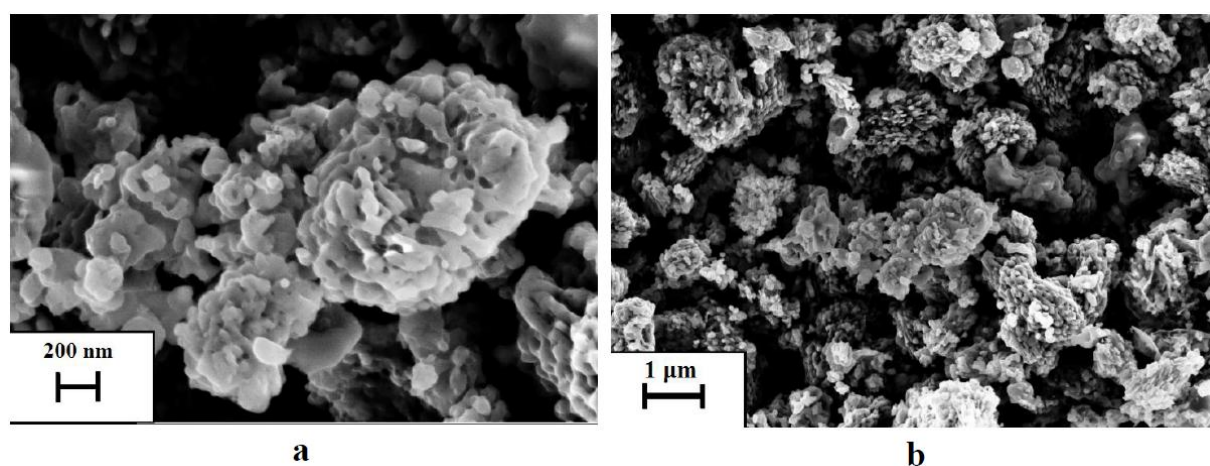
Figure 3. SEM micrographs of Li$_{0.99}$Fe$_{0.98}$Ni$_{0.01}$Cr$_{0.01}$PO$_4$/C taken at different magnification (a, b).
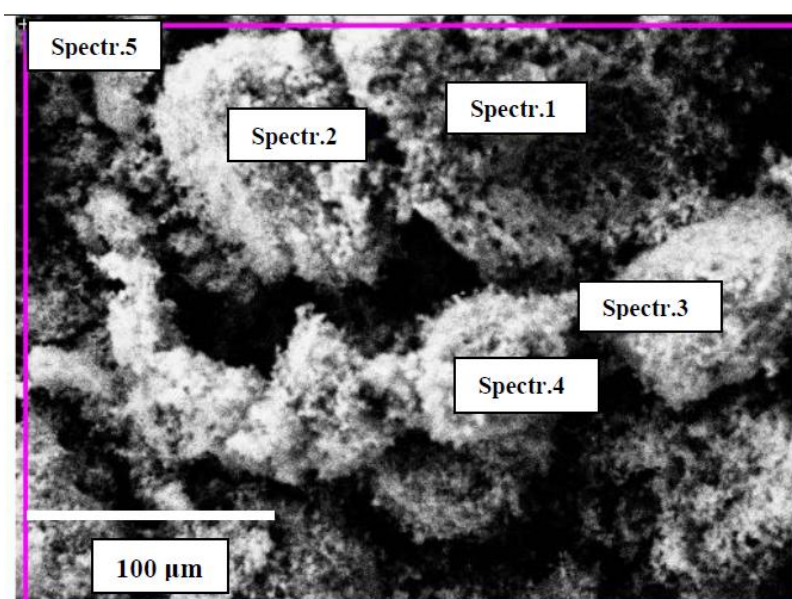
Figure 4. Electronic image of Li$_{0.99}$Fe$_{0.98}$Ni$_{0.01}$Cr$_{0.01}$PO$_4$/C, the areas where the EDX microanalysis was performed are marked with a rectangles.
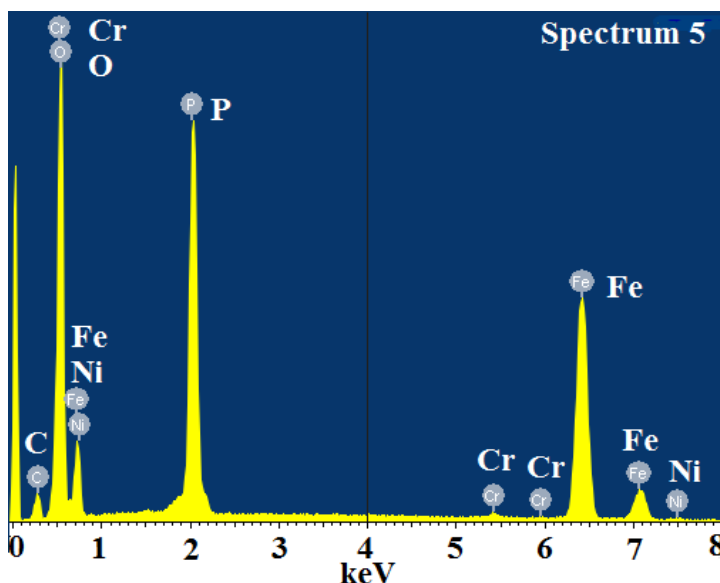
Figure 5. EDX spectrum of $Li_{0.99}Fe_{0.98}Ni_{0.01}Cr_{0.01}PO_4/C$

Table 1. The content of elements in the $Li_{0.99}Fe_{0.98}Ni_{0.01}Cr_{0.01}PO_4/C$ sample (in atomic %).

Spectrum	C	O	P	Cr	Fe	Ni
Calculated	14.3	57.1	14.3	0.14	14.0	0.14
Found	12.2	58.1	15.1	0.16	14.1	0.16
Data spread	±2.5	±8	±3	±1.5	±3	±1.5

The discharge capacity evolution of the analyzed samples during the cycling and the charge-discharge curves at the second cycle are presented in Fig. 6. At the first cycle the discharge capacity of pure lithium iron phosphate at the current density of 20 mA/g was about 147 mA/g, which is approximately 87% of the theoretical capacity of $LiFePO_4/C$. Based on the results of the cycling, it was determined that the doping of $LiFePO_4/C$ results in the lowering of its discharge capacity: thus, for the $Li_{0.99}Fe_{0.98}Cr_{0.01}Ni_{0.01}PO_4/C$ sample the discharge capacity was about 139 mAh/g.

The comparison of the charge-discharge curves of the samples of pure and doped lithium iron phosphate showed that the doping results in the shift of the charge and discharge potentials and reduction of the difference between them (ΔV): from 66 mV for $LiFePO_4/C$ to 53 mV for the doped sample at the current density of 20 mA/g (Fig. 6b). Moreover, for the $Li_{0.99}Fe_{0.98}Cr_{0.01}Ni_{0.01}PO_4/C$ sample, a minor change in the charge-discharge curve was noted at the end of discharge. It is worth mentioning that the effect of polarization diminution due to doping is documented in a number of papers. For instance, the average difference between charge and discharge voltage for $LiFe_{0.99}V_{0.01}PO_4$ is less than that for plain $LiFePO_4$ by 10 mV, and this effect is higher for higher vanadium content [14]. Similar effects are described in [21] for $LiFePO_4$ doping by Gd, and in [23] for $LiFePO_4$ doping by Mn and Ni simultaneously. In particular, it is shown that ΔV for $LiFePO_4/C$ amounts to 97 mV, whereas for doped samples $LiFe_{1-x-y}Ni_xMn_yPO_4/C$ (x=0.01, 0.02, 0.03 and 0.04; x + y = 0.05) ΔV is

equal to 65, 60, 53 and 36 mV, respectively. The effect of the polarization diminution can be explained by increase of electron conductivity of doped samples.
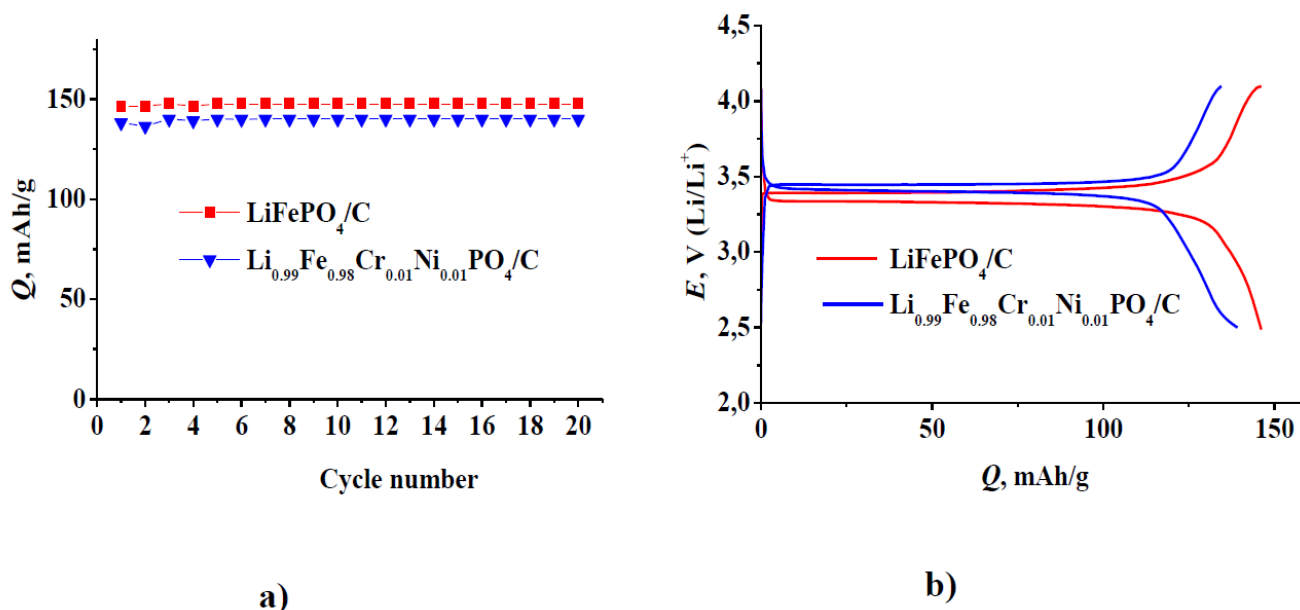
Figure 6. Change of discharge capacity during the cycling (a) and charge-discharge curves (b) of lithium iron phosphate samples. The current density is 20 mA/g.

The influence of the current density on the discharge capacity of the $LiFePO_4/C$ and $Li_{0.99}Fe_{0.98}Cr_{0.01}Ni_{0.01}PO_4/C$ samples is shown in Fig. 7. As the figure shows, the discharge capacity of $LiFePO_4/C$ at the current density of 20 mA/g exceeds the discharge capacity of $Li_{0.99}Fe_{0.98}Cr_{0.01}Ni_{0.01}PO_4/C$. However, even an insignificant increase of the current density (up to 100 mA/g) results in a sizeable reduction of the discharge capacity of $LiFePO_4/C$ and far less reduction thereof for $Li_{0.99}Fe_{0.98}Cr_{0.01}Ni_{0.01}PO_4/C$. At further increase of the current density from 20 mA/g up to 3,200 mA/g, this tendency remains, which results in the reduction of the discharge capacity by 4 times for $LiFePO_4/C$ and by 2.9 times for $Li_{0.99}Fe_{0.98}Cr_{0.01}Ni_{0.01}PO_4/C$. The influence of the current density on the discharge capacity of the samples can be demonstrated more clearly in logarithmical coordinates corresponding to the famous Peukert's equation $Q = Q_0/i^{\alpha}$. For $LiFePO_4/C$ and $Li_{0.99}Fe_{0.98}Cr_{0.01}Ni_{0.01}PO_4/C$, the dependence of lg$Q$ on lg$i$ is broken up into two sections. The α index at low current density for both samples turned out to be approximately identical and amounted to some 0.19 for $LiFePO_4/C$ and 0.14 for the doped sample. At higher current density, the α index increased up to 1.1 for $LiFePO_4/C$ and 0.36 for $Li_{0.99}Fe_{0.98}Cr_{0.01}Ni_{0.01}PO_4/C$. The physical meaning of the α index for two-phase electrodes is subject to a particular examination. It is worth noting that the general result of the present work on beneficial effect of $LiFePO_4$ doping agrees by and large with results documented in [9–22]. Indeed, all these papers report on enhancement of discharge capacity of doped $LiFePO_4$ at rather high currents (> 3C-rate). For instance, recalculation of data of [22] gives the α value as low as 0.11 for $Li_{0.97}FeCr_{0.01}PO_4/C$ at low discharge current. Recalculation of data [23] for $LiFe_{0.95}Ni_{0.02}Mn_{0.03}PO_4/C$ gives α values 0.05 for currents less than 2C-rate and 0.14 for currents from 2C-rate to 10C-rate. At the same time α values for non-doped $LiFePO_4$ were equal to 0.08 and 0.19 for

low and high C-rates. The doping of LiFePO$_4$ by magnesium leads to decrease of α from 0.18 to 0.05 and from 1.5 to 0.29 for different current densities [15]. Therefore these results confirm our conclusion about complex character of *Q* vs. *i* dependence with different α index in different current ranges.

As to the irreversible capacity at the first cycle, calculated by the difference between the charge and discharge capacity, for undoped lithium iron phosphate and the doped Li$_{0.99}$Fe$_{0.98}$Cr$_{0.01}$Ni$_{0.01}$PO$_4$/C sample the irreversible capacity was about 5% of the reversible capacity, which is conditioned by oxidation of the electrolyte with the formation of a solid electrolyte interface.

Degradation during the cycling of undoped lithium iron phosphate was about 0.1 % per cycle. For the doped sample this value was less than 0.05%. The similar results were reported in [23], namely capacity loss was about 0.08% per cycle for non-doped lithium iron phosphate and less than 0.015% for LiFe$_{0.95}$Ni$_{0.02}$Mn$_{0.03}$PO$_4$/C. Authors [15] reported that the capacity loss ratio was 47.2% after 300 cycles of pure LiFePO$_4$ sample and the capacity loss ratio was 2.9% after 300 cycles of LiFe$_{0.96}$Mg$_{0.04}$PO$_4$/C sample. The good cycle behavior is mainly ascribed to the enhancement of the electronic conductivity of sample due to doping together with almost uniform carbon coating.
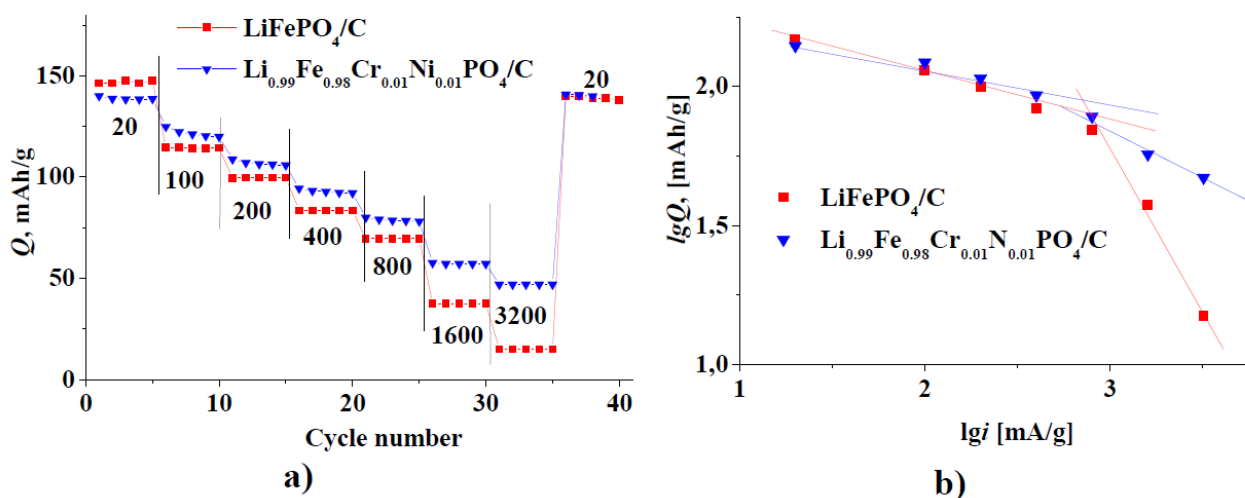
Figure 7. Change of discharge capacity during the cycling (a) and dependence of discharge capacity on the current density in logarithmic coordinates (b) for lithium iron phosphate samples. Current density in [mA/g] is shown in the Fig. 7a.

The cyclic voltamograms of the Li$_{0.99}$Fe$_{0.98}$Cr$_{0.01}$Ni$_{0.01}$PO$_4$/C sample, obtained at various potential scan rates (*v*), are given in Fig. 8. The shapes of these curves are similar to that reported in [12, 13, 15, 18, 20]. One can see strongly pronounced peaks in anodic and cathodic areas.

The increase of the *v* results in the increase of the currents in the maximum of the voltamogram, both in the cathode and anode regions, and some shift of the potential of the maximum to the anode and cathode sides for lithium extraction and insertion processes, accordingly. The discharge capacity, calculated from the area under the curve during the cathode half-cycle at the potential scan rate of 0.1 mV/s, was 137.3 mA/g, which is well agreed with the results of the galvanostatic cycling.
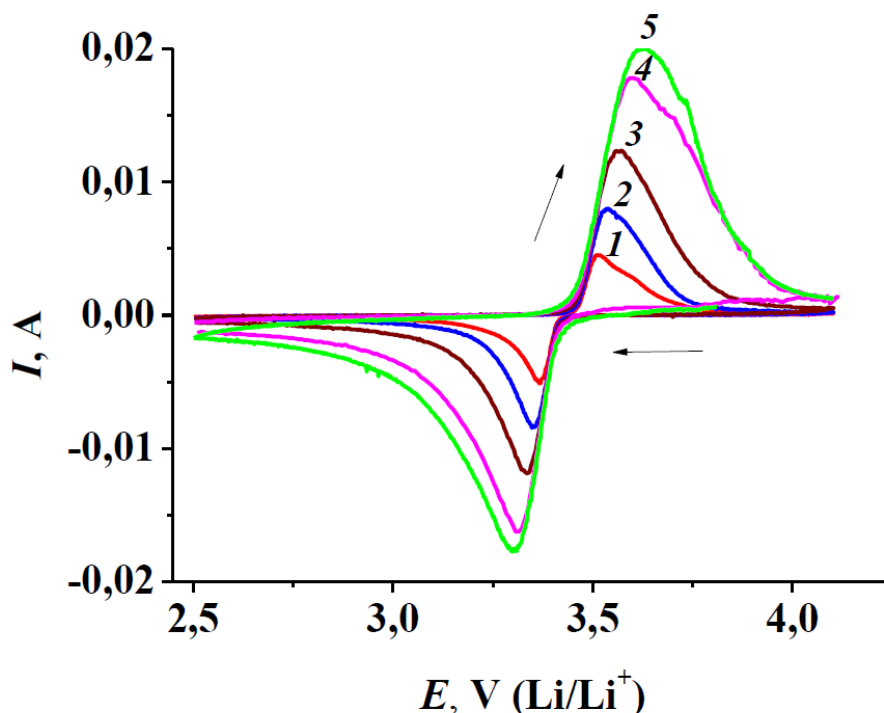
Figure 8. The cyclic voltamograms of $Li_{0.99}Fe_{0.98}Cr_{0.01}Ni_{0.01}PO_4/C$ sample. Potential scan rates (V/s): 1 – 0.0001, 2 – 0.0002, 3 – 0.0004, 4 – 0.0008, 5 – 0.001. Weight of the sample is 0.015 g. Visible area of the electrode surface is 2.25 cm^2.

The current dependence in the cathode maximum at the potential scan rates of 0.1, 0.2, 0.4, 0.8 and 1 mV/s in the coordinates $I_p = f(v^{1/2})$ is shown in Fig. 9. The dependence goes through the origin of coordinates, which evidences of meeting the condition of semi-infinite linear diffusion. Formally, this dependence can be considered satisfying the Randles–Sevcik equation that for the temperature of 25°C and diffusion of a single-charged particle is as follows:

$$I_p = 2.69 \cdot 10^5 \, ScD^{1/2}v^{1/2} \qquad (2)$$

where S is true area of electrode surface, c is initial concentration of diffusing material, mole/cm^3, D is its diffusion coefficient, cm^2/s, and v is potential scan rate, V/s, and numerical coefficient has dimensions $A*s*mole^{-1} V^{-1/2}$. Exactly the same approach was used, e.g. in the papers [12, 13, 18, 24–27]. However, the equation (2) was derived on the assumption that the electrode potential depends on the concentration of the diffusing material under the Nernst equation, i.e. assuming that the activity coefficient of the potential-determining material is strictly equal to one. Objectively, the activity coefficient of diffusing lithium differs markedly from unity. Moreover, when deriving the equation (2), it was assumed that the diffusion coefficient does not depend on the concentration of the diffusing material, while in the two-phase system under discussion it is far from being the case. In the present paper, the approach suggested in the paper [28, 29] was used to analyze voltammetric results. The dependence of the potential on the lithium concentration is described in this case by the updated Nernst equation

$$E = E_0 + (RT/znF)\ln c \qquad (3)$$

where z is adjustable parameter.

The correctness of such approach is proved by the fact that the cathode curve of galvanostatic lithiation, obtained at a relatively low current, with sufficient approximation is linearized in the coordinates *E*, lg*c* in the interval of working potentials (Fig. 10). In this case, the equation (2) should be replaced with the updated equation

$$I_p = 2.69*10^5 \, S c z^{1/2} D^{1/2} v^{1/2} \tag{4}$$
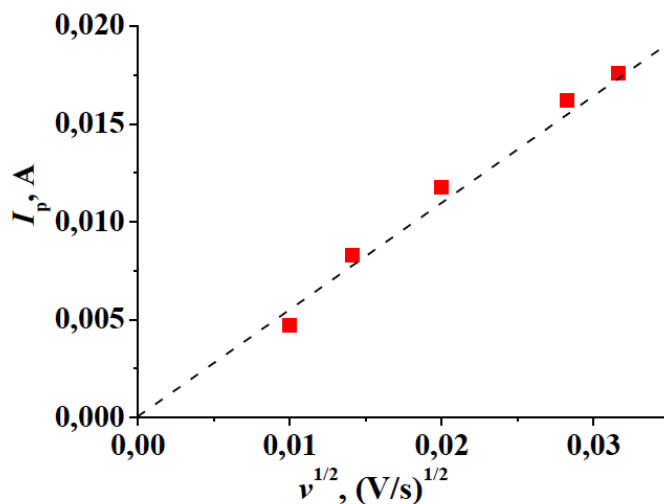
Figure 9. Dependence of the cathode current in the maximum of the voltamogram on the square root of the potential scan rate.
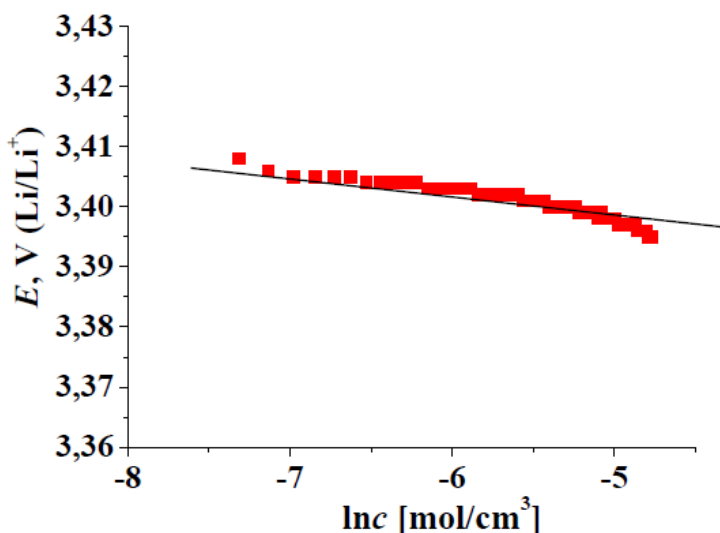
Figure 10. Dependence of the electrode potential based on $Li_{0.99}Fe_{0.98}Cr_{0.01}Ni_{0.01}PO_4/C$ on the lithium concentration (cathode curve adjustment)

The slope of straight line in Fig. 10 and equation (3) imply that $z = 6.68$. The lithium concentration is 0.02 mole/cm^3. The slope of the straight line in Fig. 9 is 0.22 $*A *s^{1/2} *V^{-1/2}$. The visible area of the electrode is 2.25 cm^2. There is considerable uncertainty as to how the true area of the surface on which the diffusion occurs might be assessed. The characteristic crystallite size of the

material being studied amounts to dozens of nanometers. The size of agglomerates can be assessed (by order of magnitude) as 1 μm. In this case, the diffusion front surface is 150 cm^2.

Calculation using the equation (4) in such case estimates $D \approx 1.2 \cdot 10^{-14}$ cm^2/s, which is agreed for instance with the values obtained in [23, 27, 29, 33, 38]. It should be emphasized that the so calculated lithium diffusion coefficient represents a certain effective value that corresponds to the situation of particle diffusion in isotropic media. The longest diffusion time in the described voltammetric experiments (at the minimum potential scan rate) is 16,000 s. It corresponds to the depth of the front diffusion penetration $\approx 5 \cdot 10^{-5}$ cm, which is 10 times less than the characteristic particle size, and does not contradict the assumed plane semi-infinite geometry of the diffusion. It is high time to stress the fact that a wide range of lithium diffusion coefficient in LiFePO$_4$ (from 10^{-15} to 10^{-11} cm^2/s) have been reported [12, 13, 18, 24–39]. The lack of consistency in literature is likely to be caused by wide variety of synthesis conditions, as well as by errors in diffusion coefficients measurements.

4. CONCLUSIONS

As can be seen from the above, the doping of lithium iron phosphate with trivalent cations of chromium and nickel results in the increase of the discharge capacity at high discharge rates with the simultaneous stability augmentation during the cycling. This effect, at partially, least can be explained by the enhanced electronic conductivity of the material and reduced size of particles in the synthesized material.

References

1. R. R. Zhao, G. Z. Ma, L. C. Zhu, A. J. Li, H. Y. Chen, *Int. J. Electrochem. Sci*., 7 (2012)10923-10932.
2. A. Naik, J. Zhou, C. Gao, L. Wang, *Int. J. Electrochem. Sci*., 9 (2014) 6124-6133.
3. J. Liu, X. Zhang, R. Wang, J. Zhang, *Int. J. Electrochem. Sci*., 7 (2012) 12983-12991.
4. N. Zhou, E. Uchaker, Y.-Y. Liu, S.-Q. Liu, Y.-N. Liu, G.-Z. Cao, *Int. J. Electrochem. Sci.*, 7 (2012) 12633-12645.
5. J. Song, G. Shao, Z. Ma, G. Wang, J. Yang, *Electrochim. Acta*, 178 (2015) 504-510.
6. M. Chen, L.-L. Shao, H.-B. Yang, Q.-Y. Zhao, Z.-Y. Yuan, *Electrochim. Acta*, 168 (2015) 59-68.
7. N. Vicente, M. Haro, D. Cíntora-Juárez, C. Pérez-Vicente, J. L. Tirado, S. Ahmad, G. Garcia-Belmonte, *Electrochim. Acta*, 163 (2015) 323-329.
8. R. Mei, Y. Yang, X. Song, Z. An, J. Zhang, Electrochim. Acta, 153 (2015) 523-530.
9. Y. Mi, C. Yang, Z. Zuo, L. Qi, C. Tang, W. Zhang, H. Zhou, *Electrochim. Acta,* 176 (2015) 642-648.
10. Y. Lin, Y. Lin,, B. Zeng, G. Zhao, T. Zhou, M. Chen, X. Mao, H. Lai, Z. Huang, *Int. J. Electrochem. Sci.,* 6 (2011) 6653-6661.

11. S. Novikova, S. Yaroslavtsev, V. Rusakov, A. Chekannikov, T. Kulova, A. Skundin, A. Yaroslavtsev, *J. Power Sources*, 300, (2015) 444-452.
12. M. Chen, L. Shao, H. Yang, T. Ren, G. Du, Z. Yuan, *Electrochim. Acta*, 167 (2015) 278-286.
13. M. Vujković, D. Jugović, M. Mitrić, I. Stojkovic, N. Cvjetićanin, S. Mentus, *Electrochim. Acta*, 109 (2013) 835-842.
14. M.-S. Chen, S.-H. Wu, W. K. Pang, *J. Power Sources, 241*, (2013), 690–695.
15. A. Örnek, O. Efe, *Electrochim. Acta*, 166 (2015) 338-349.
16. C. Hu, H. Yi, H. Fang, B. Yang, Y. Yao, W. Ma, Y. Dai, *Int. J. Electrochem. Sci.,* 5 (2010) 1457-1463.
17. R. Qing, M. Yang, Y. Meng, W. Sigmund, *Electrochim. Acta*, 108 (2013), 827-832.
18. H. Gao, L. Jiao, J. Yang, Z. Qi, Y. Wang, H.Yuan*, Electrochim. Acta*, 97 (2013) 143-149.
19. H. Gao, L. Jiao, W. Peng, G. Liu, J. Yang, Q. Zhao, Z. Qi, Y. Si, Y. Wang, H. Yuan, *Electrochim. Acta*, 56 (2011) 9961-9967.
20. J. Z. Li, S.Y. Wang, L. H. Wei, Z. Liu, Y. W. Tian, *Int. J. Electrochem. Sci.,* 10 (2015) 6135-6145.
21. L. Pang, M. Zhao, X. Zhao, Y. Chai, *J. Power Sources,* 201 (2012) 253–258.
22. J. Ying, M. Lei, C. Jiang, C. Wan, X. He, J. Li, L. Wang, J. Ren, *J. Power Sources,* 158 (2006) 543-549.
23. H. Shu, X. Wang, Q. Wu, B. Hu, X. Yang, Q. Wei, Q. Liang, Y. Bai, M. Zhou, C. Wu, M. Chen, A. Wang, L. Jiang, *J. Power Sources,* 237, (2013) 149-155.
24. L. B. Chen, J. Y. Xie, H. C. Yu, T. H. Wang, *Electrochim. Acta*, 53 (2008) 8149-8153.
25. E. Avci, *J. Power Sources,* 270 (2014) 142-150.
26. R. Chen, Y. Wu, X.Y. Kong, *J. Power Sources*, 258 (2014) 246-252.
27. X. Zeng, Q. Liu, M. Chen, L. Leng, T. Shu, L. Du, H. Song, S. Liao, *Electrochim. Acta*, 177 (2015) 277-282.
28. A. V. Churikov, A. V. Ivanishchev, I. A. Ivanishcheva, K. V. Zapsis, I. M. Gamayunova, V. O. Sycheva, *Russ. Journal of Electrochemistry*, 44 (2008) 530-542.
29. A. V. Ivanishchev, A. V. Churikov, A. V. Ushakov, *Electrochim. Acta,* 122 (2014) 187-196.
30. S. M. Zhang, J. X. Zhang, S. J. Xu, X. L. Yuan, B. C. He, *Electrochim. Acta*, 88 (2013) 287-293.
31. K. Tang, X. Yu, J. Sun, H. Li, X. Huang, *Electrochim. Acta,* 56 (2011) 4869-4875.
32. P. P. Prosini, M. Lisi, D. Zane, M. Pasquali, *Solid State Ionics,* 148 (2002) 45-51.
33. Y.-R. Zhu, Y. Xie, R.-S. Zhu, J. Shu, L.-J. Jiang, H.-B. Qiao, T.-F. Yi, *Ionics,*17 (2011) 437-441.
34. H. Manjunatha, T. V. Venkatesha, G. S. Suresh, *Electrochim. Acta,* 58 (2011) 247-257.
35. Z. Ma, G. Shao, X. Qin, Y. Fan, G. Wang, J. Song, T. Liu, *J. Power Sources,* 269 (2014) 194-202.
36. Y.-F. Wu, Y.-N. Liu, S.-W. Guo, S.-N. Zhang, T.-N. Lu, Z.-M. Yu, C.-S. Li, Z.-P. Xi, *J. Power Sources,* 256 (2014) 336-344.
37. D. Lepage, F. Sobh, C. Kuss, G. Liang, S.B. Schougaard, *J. Power Sources,* 256 (2014) 61-65.
38. C.-T. Hsieh, C.-T. Pai, Y.-F. Chen, P.-Y. Yu, R.-S. Juang, *Electrochim. Acta,* 115 (2014) 96-102.
39. J. Hea, J. Wanga, H. Zhonga, J. Dingc, L. Zhanga, *Electrochim. Acta,* 182 (2015) 900-907.